International Journal of Solids and Structures 147 (2018) 29–39

Contents lists available at ScienceDirect

International Journal of Solids and Structures

journal homepage: www.elsevier.com/locate/ijsolstr

Micro-crack damage in strip of fracture process zone

Wang Limin[a], Li Xia[a], Xu Shilang[b,*], Wang Haiying[c], Zhang Zhaojun[a]

[a] Science School, Qingdao University of Technology, Qingdao Shandong 266033 China
[b] College of Civil Engineering and Architecture, Zhejiang University, Yuhangtang Road 866, Hangzhou 310058 China
[c] LNM of the Institute of Mechanics, Chinese Academy Sciences, Beijing 100190, China

ARTICLE INFO

Article history:
Received 24 October 2017
Revised 12 March 2018
Available online 18 April 2018

Keywords:
Quasi-brittle materials
Micro-crack
Damage factor
Fracture process zone
Multi-scale mechanics
Cohesive crack model

ABSTRACT

Damage and fracture of quasi-brittle materials are non-reversible processes of micro-defects and micro-cracks, often accompanied by a strip of micro-crack damage along the end of the macro-crack or gap. In this work, the micro-crack damage parameters in the strip are calculated, and a mechanics model is proposed to analyze the relation between deformation and force. The mechanics parameters are also determined using meso-mechanics homogenization of the damage zone of the micro-crack strip. Then, calculations of the deformation and stress in the damage strip are introduced, and the damage factor is estimated using a cohesive crack model. Finally, the relationship between the micro-crack and macro-fracture zone is correlated to electron microscopy data of a cast iron specimen and numerical results. For the damage factor, damage density, and geometrical factors of micro-cracks, the meso-mechanics scale is correlated to macro-mechanics in the damage fracture process zone by combining the homogenization method and cohesive crack model of nonlinear fracture.

1. Introduction

The failure of engineering materials is affected by many factors, especially the strength and durability of the material. Therefore, evaluation of the stress and deformation, structural bearing capacity, and damage fracture are critical (Roth et al., 2014; Hertzberg, 1996) . With the gradual improvement of modern characterization tools, the visual resolution of material deformation as a function of force can now be finely tuned. The meso-mechanics theories developed over the past dozens of years have laid a solid foundation for the study of material behavior (Yang and Lee,1993; Carpinteri et al., 2006; Zhou and Li, 2015) . With improvements of computational equipment and methods, mechanical analysis of the material and structure failure has become increasingly accurate (Yao et al., 2015) . In addition, a series of discussions on the fracture of various metals was recently held, which is the “The Sandia Fracture Challenge” (Boyce et al., 2014).

Quasi-brittle materials, which release a small strain energy before failure, are generally thought to contain microscopic defects or numerous micro-cracks. Thus, the deformation mechanism of microscopic defects is of particular concern in these materials. The fracture mechanics that addresses geometrical cracks of solids and the micro-damage mechanics based on the theory of continuous medium theory have been well developed in recent decades. For example, the mechanism of a plastic strain gradient was used in the analysis of a steady-state crack growth in response to fracture (Wei et al., 2004). The nucleation of micro-cracks and crack propagation have also been analyzed for thermal shock (Cyron et al., 2014). An analysis of the interactions of multiple micro-cracks was presented by Zhan et al. (1999). Nanotechnology was also introduced in solid mechanics by Li (1998). The effects of the micro-crack density on the flexibility and damage tensor were investigated in a micro-cracked medium, and the mechanical behavior of hybrid materials was also investigated (Krajcinovic,1984; Huang et al., 2016; Feng and Yu, 2002). However, certain problems related to material damage have not yet been addressed because of the unknown relationship between micro-cracks and damage variables. Few studies on the organic connection of macroscopic fracture and microscopic defect damage have been reported. Thus, the multi-scale issue, including micro-crack damage to macro-fracture, has been one of the long-term research interests of the Chinese State Key Laboratory of Nonlinear Mechanics.

Compared with ductile materials that are pure and integrated, quasi-brittle materials more likely contain impurities and defects as well as micro-cracks or tiny pores. Material defects and micro-cracks can easily expand when the media is loaded with stress or deformation. As a crack forms in the high-stress area of materials, the local bearing capacity will be reduced after crack nucleation (Pichler and Hellmich, 2010; Gao, 1989). A damage strip or fracture process zone often appears at the tip of a smooth crack.

* Corresponding author.
E-mail addresses: wanglimin@qut.edu.cn (W. Limin), slxu@zju.edu.cn, shilangxu98@sina.com (X. Shilang).

https://doi.org/10.1016/j.ijsolstr.2018.04.008
0020-7683/

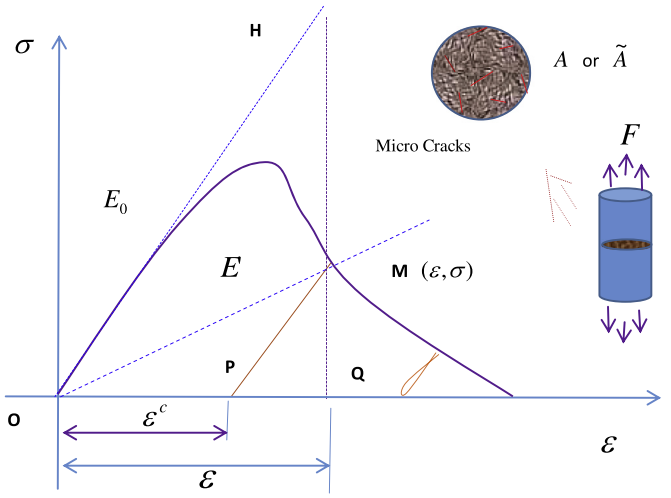

Fig. 1. Schematic stress–strain curve for the loading process.

Hillerborg et al. (1976) used a virtual crack model to study the fracture properties of concrete. In addition, Xu et al. (1999) performed cracking experiments and fracture criterion analysis of concrete to establish a double-K fracture model. For cast iron, a strip of micro-cracks was found at the tip of macroscopic crack (Wang et al., 2008; Shackelford, 2000). In this work, an approach is proposed to connect micro-crack damage with the macro-fracture process using a combination of a meso-mechanics approach and nonlinear fracture model.

2. Damage and fracture of solid with applied stress

2.1. Damage factor

To explain the deformation of a material with force and its inner micro-structural changes, Kachanov and Rabotnov first presented the damage factor using an analytical method of continuum plasticity and creep deformation. The definition of the damage factor was correlated to the effective section area bearing load (Krajcinovic, 1984; Feng and Yu, 2002). If the initial section area of some solid or undamaged section is A, the effective area is $\tilde{A}$ in some state. When the material is damaged by stress, the damage factor D can be calculated as follows:

$$D = 1 - \frac{\tilde{A}}{A} \tag{1}$$

where, $\tilde{A} = A$ and $D = 0$ for the undamaged material, $\tilde{A} = 0$ and $D = 1$ for the completely damaged material. When micro-cracks appear in the cross section and the bearing area is reduced, the damage variable D is usually between 0 and 1. In the state of single-axis tensile stress for a quasi-brittle material, only one peak appears in the stress σ vs strain ε curve, as shown in Fig. 1. The values of (σ, ε) are set according to the initial configuration. For the purpose of objectivity for force F, the equivalent stress $\tilde{\sigma}$ is introduced:

$$F = \tilde{\sigma}\tilde{A} = \sigma A \tag{2}$$

The stress–strain relationship is specified by

$$\sigma = E'A \tag{3}$$

Where E' is the nominal elastic (Young's) modulus. If the initial undamaged elastic modulus of the media is E_0, the ratio E'/E_0 represents the damage of the material. Without loss of generality, the material state is considered at point "M," with coordinates (ε, σ), as shown in Fig. 1. In addition, the total strain ε is the sum of the elastic strain ε^e and the non-elastic strain ε^c:

$$\varepsilon = \varepsilon^e + \varepsilon^c \tag{4}$$

Here, $\varepsilon^e = \sigma/E_0$ for the line segment "PQ." The total strain ε can be correlated to the effective stress $\tilde{\sigma}$ (defined as the vertical coordinate of point "H" in Fig. 1) using the following equation:

$$\tilde{\sigma} = E_0\varepsilon \tag{5}$$

Substituting Eqs. (3) and (5) into Eq. (2), the damage variable D can be written as

$$D = 1 - \frac{\tilde{A}}{A} = 1 - \frac{\sigma}{\tilde{\sigma}} = 1 - \frac{E'}{E_0} \tag{6}$$

When the initial strain does not exceed the elastic limit, $E' = E_0$ and $D = 0$. When the strain exceeds the elastic limit, the value of the nominal elastic modulus E' gradually decreases and approaches zero. The material fails or breaks when $E' = 0$and $D = 1$. Fig. 1 shows that triangle "QPM" is similar to triangle "QOH." Taking Eq. (4) into account,

$$D = 1 - \frac{\sigma}{\tilde{\sigma}} = 1 - \frac{\varepsilon^e}{\varepsilon} = \frac{\varepsilon^c}{\varepsilon} \tag{7}$$

which indicates that the damage variable can be calculated based on the inelastic strain and total strain. This equation is similar to the expression of equivalent strain or stress about damage factor (Lemaitre, and Chaboche,1990; Shen, 1995).

2.2. Damage strip of a fracture process zone

Unlike a ductile material, micro-cracks and defects are often observed in a quasi-brittle material under stress and deformation before structure failure. The damage zone contains many types of defects or micro-cracks. In fracture mechanics, the damage zone is simplified as a virtual cohesive crack (Hillerborg et al., 1976; Bouvard et al., 2009). The cohesive force along this virtual crack reveals the existence of medium interaction in the damage zone. Fig. 2 presents a schematic diagram of the mechanics model. The micro-cracks appear in the damage zone at the end of a macro-crack. It is different from the analysis model of a penny-shaped cohesive micro-crack proposed by Pichler and Dormieux (2007,2009). For the reason of simplicity, the cohesive segment at each micro-crack tip is not involved in this proposed damage strip model.

Regarding the fictitious cohesive crack model (FCCM) at the tip of a macro smooth crack, as shown in Fig. 2, the strip length of the damage zone Γ is simplified into a cohesive crack segment with some stress distribution ($\hat{\sigma}_{yy}$). When the damage zone length is not too long with respect to the length of the smooth macro-crack, the cohesive stress and fictitious crack opening displacement (δ) distributed along the virtual crack segment can be estimated based on the stress intensity factor K_I of the macro-crack with far loading field. According to the principle of solid mechanics and the solution of integral equation (Wang et al., 2006; Shen, 2002; Polyanin and Manzhirov, 1998), the FCOD can be written as a polynomial of different power exponents for the distance of the position from the macro-crack tip. On the basis of the solution of the integral equation of the opening displacement and cohesion stress, algebraic equations for determining the coefficients were obtained using a variational method. However, there was only one non-zero term for the first two terms, and the third and higher terms were not convenient (Smith, 1994; Zhang et al., 2012). In the Appendix of this paper, the following expression for δ with its cohesive stress is derived:

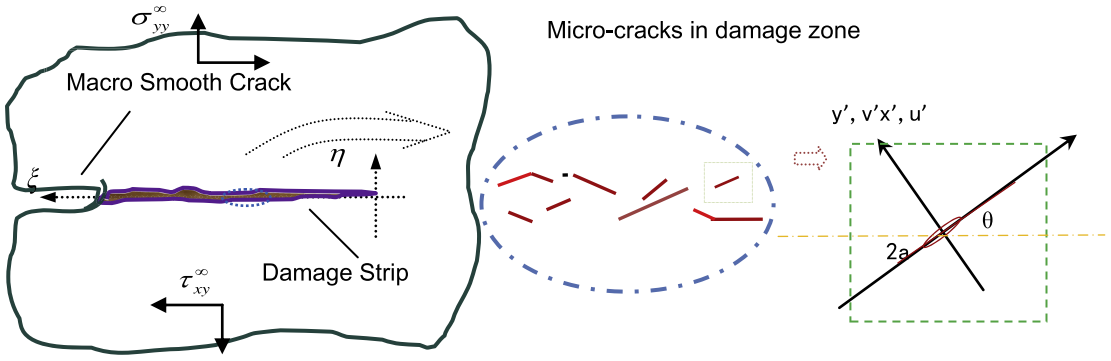

Fig. 2. Schematic diagram of a micro-crack damage strip at the tip of a macroscopic crack.

$$\delta(\xi) = \frac{16K_{\mathrm{I}}}{3E}\sqrt{\frac{\Gamma}{2\pi}}\left(\frac{\xi}{\Gamma}\right)^{3/2};\hat{\sigma}(\xi)$$
$$= \frac{K_{\mathrm{I}}\sqrt{2}}{\sqrt{\pi\Gamma}}\sqrt{\frac{\Gamma-\xi}{\Gamma}};(0\le\xi\le b) \quad (8a,b)$$

Here, ξ is the distance from any point in the damage zone to the smooth crack tip point, as illustrated in Figs. A1 and 2.The K_I is the stress intensity factor (SIF) of tension loaded far from the crack tip. The opening displacement and stress distribution of cohesive crack model Eq. (8) is correlated to the observation of mortar FPZ by laser speckle technique (Horii and Ichinomiya, 1991). As shown in Fig. A2, it can be known that the analysis model is validated for quasi-brittle materials.

If value of K_{I} in Eqs. (8a,b) is between the initiation SIF and instability SIF, as $K_{\mathrm{Ic}}^{\mathrm{ini}} \le K_{\mathrm{I}} \le K_{\mathrm{Ic}}^{\mathrm{un}}$, the propagation of macro crack is quasi static, according to the double-K model of concrete fracture proposed by Xu and Reinhardt (1999). In other words, the crack is not extending if the SIF of far load is less or equal to the resistance SIF ($K_{\mathrm{I}} \le K_{\mathrm{R}}$). In this sense, the K_{I} may be the resistance SIF (K_R) for some stability statue, and it must be less than the fracture toughness of its material structure. As the extending of FPZ length near a macro-crack tip, the value of K_R is increasing usually, but it is limited. So the quasi static development of K_{I} is an alternate process of equilibrium or non-equilibrium for K_I and K_R. Then, the value of K_{I} should be less than its fracture toughness ($K_{\mathrm{Ic}}^{\mathrm{un}}$).

By the way, if $\xi \to 0$ in Eq. (8b), the cohesive stress should approach to the material ultimate tension strength, as $\hat{\sigma} \le f_t$. Some relation can be worked out among the damage length (Γ), SIF and f_t. The relationship may be concerned with crack development, when $\hat{\sigma} \ge f_t$ or the value of far loaded K_{I} is more than K_{R}. Probably, the fracture toughness can be calculated by the maximum value of K_R for some quasi-brittle material, and no too discussion is concerned in the paper. Now, let us investigate the damage issue mentioned before with regard to FPZ.

Using modern optical equipment, the opening displacement distribution of a virtual crack segment (FPZ) at the macro-crack end of concrete can be measured using the laser speckle technique, as described by Horii and Ichinomiya (1991). For another quasi-brittle material, cast iron, the fracture process was examined using a digital image correlation approach in a laser facility, and both FCOD and the strain distribution were presented in the damage strip at the pre-crack tip (Dai et al., 2013). For the FCCM framework, the width of the damage strip is not considered; however, the damage strip width is actually non-zero.

On the basis of the homogenization method, the displacement δ between both sides of the virtual crack can be considered as the deformation of the damage strip at the end of a smooth macro-crack. If elastic deformation is ignored, the displacement of the damage strip in the vertical direction of the smooth macro-crack line would be the sum of the deformation across the high-strain band of the non-elastic area. The inelastic deformation of the fracture process zone includes cavity expansion, initiation of micro-crack growth, and plastic deformation. The area around the damage strip is surrounded by elastic media. In the vertical direction of the macro-crack line, if the width of the damage band is as h, the average strain of the damage band is ε^c.The relationship between these parameters can be expressed as

$$\delta(\xi) = \varepsilon^c h(\xi) \quad (9)$$

Here, the damage strip width $h(\xi)$ varies with the distance from the macro-crack tip.

Substituting Eqs. (8) and (9) into Eqs. (6) and (7), we obtain the following expression for the damage factor:

$$D = \frac{\varepsilon^c}{\varepsilon} = \frac{\delta(\xi)/h(\xi)}{\hat{\sigma}(\xi)/E'} = \frac{\delta(\xi)E_0(1-D)}{\bar{\sigma}(\xi)h(\xi)} \quad (10)$$

Therefore, the damage factor can be written as

$$D(\xi) = \frac{\delta(\xi)E_0}{\bar{\sigma}(\xi)h(\xi)+\delta(\xi)E_0} \quad (11)$$

It is apparent that $D \to 0$ as δ approaches zero. In the damage zone, when the cohesive stress approaches zero ($\hat{\sigma} \to 0$), the damage factor of the position function approaches 1 ($D \to 1$). This formula reveals that the damage factor D of the fracture process strip is related not only to the virtual crack opening displacement and cohesive stress but also to the width of the damage zone $h(\xi)$.

2.3. Damage factor for ultimate tensile stress

If $\tilde{A}$ is the effective area of the damage zone, f_t is the ultimate tensile stress, A is the lossless or initial area, and the force applied to the effective area is $F' = A\sigma = \tilde{A}f_t$. The force F' in the non-damage area A can be expressed as $F_t = f_t A$, if it is in a state of ultimate tensile stress. When the effective area $\tilde{A}$ takes the maximum tensile stress f_{t}, the damage factor can be written as

$$D = 1 - \frac{\tilde{A}}{A} = 1 - \frac{\sigma}{f_t} \quad (12)$$

The damage variable is only correlated to the stress of the associated area. The trend of the damage factor in the fracture process zone is consistent with those described in Eqs. (1) and (6). In addition, it should be emphasized that the stress in Eq. (12) is applicable in the damaged area.

3. Stress and deformation of micro-cracks

The macroscopic mechanics parameters of stress, strain, and displacement are the result of homogenization of the internal force

and deformation of certain units. The analysis of the relationship between micro-defects or micro-cracks and macro-mechanics parameters has promoted the development of the field of meso-mechanics in solid mechanics (Feng and Yu, 2002; Zhang and Zhang, 2008; Pichler, Hellmich, 2010). With loading, the media mechanical response to one or more micro-cracks or defects is an important focus of the analysis of micro-mechanics on a representative volume element (RVE). To understand the deformation near a micro-crack in the damage zone, an analytical model can be established for a single micro-crack or multiple cracks in a solid medium, as shown in the right part of Fig. 2.

3.1. Stress and deformation around a single crack

For a single micro-crack, the coordinates parallel and perpendicular to the crack axial direction are (x', y'), respectively, and the corresponding displacements are (u', v') at a certain point near the crack. The normal stress and shear stress near a single micro-crack are signed in the right field of Fig. 2 for (σ', τ'), respectively, and either far-field stress $(\sigma_{yy}^{\infty}, \tau_{xy}^{\infty})$ direction is perpendicular or parallel to the axis of the macro-crack. If the micro-crack of the damage zone is not parallel to the axes of the macro-crack, the angle θ is between the micro-crack and macro-crack axes, as shown in the right of Fig. 2. Coordinate transformation, including sin θ or cos θ, is needed for plane problems of micro-cracks. In addition, the stress and displacement fields of a crack can be divided into type I and II in fracture mechanics.

For a center crack of length $2a$, when a uniaxial tensile stress is applied perpendicular to its axes and the shear stress is zero about the crack $\theta = 0$. The stress and displacement fields can be determined using Westergard's stress function $\Phi = \bar{\bar{Z}}_I(z) + y\,\mathrm{Im}\bar{Z}_I(z)$, if the bi-harmonic equation $\nabla^4\Phi = 0$ is satisfied by the far-field boundary conditions of the crack (Tada et al., 2000). Here, $\bar{Z}_I(z)$ and $\bar{\bar{Z}}_I(z)$ are, respectively, the one-time or two-time integral of the analytical function. If the analytical function of a type-I crack is $Z_I(z) = \sigma.z/\sqrt{z^2 - a^2}$ under uniaxial tension σ, the displacements in the x and y direction are (u, v), respectively. This situation is expressed in the plane-stress condition as

$$u_I = \left[(1-\nu)\mathrm{Re}\bar{\bar{Z}}_I - (1+\nu)y\,\mathrm{Im}Z_I\right]/E \tag{13a}$$

$$v_I = \left[2\mathrm{Im}\bar{\bar{Z}}_I - (1+\nu)y\,\mathrm{Re}Z_I\right]/E \tag{13b}$$

In addition, the field of a type-II crack in the plane-strain state formed by shear stress τ can be expressed as follows:

$$u_{II} = \left[(1+\nu)[2(1-\nu)\mathrm{Im}\bar{Z}_{II} - y\,\mathrm{Re}Z_{II}\right]/E \tag{13c}$$

$$v_{II} = \left[(1+\nu)[-(1-2\nu)\mathrm{Re}\bar{\bar{Z}}_{II} - y\,\mathrm{Im}Z_{II}\right]/E \tag{13d}$$

Here, $Z_{II}(z) = \tau.z/\sqrt{z^2 - a^2}$ is an analytical function of a type II crack that satisfies the bi-harmonic equation and boundary conditions, and E is the Young's modulus. The deformation field of a single crack can be determined using the integral or derivative of a complex analytical function in polar coordinates. On the basis of the above formula, it is not difficult to determine the displacement or deformation distribution near a crack under various loading conditions.

3.2. Macro strain calculation for damage zone with micro-cracks

For the analysis of material behavior from the microscopic to macroscopic view, the homogenization method of solid mechanics is an effective mean approach. The material under the macro-frame can be considered as a mixture of micro-elements. On the basis of the universal relation criterion of force and energy, scholars have established different analytical methods, including the self-consistent scheme, variational approach, differential method, and Mori–Tanaka method (Zhang and Zhang 2008; Hashin and Shtrikman, 1962). For the micro-crack damage of quasi-brittle materials, the effect of micro-crack propagation on macroscopic flexibility was investigated by Krajcinovic (1984). Micro-cracks are not uniformly distributed in the damage zone of actual materials. In addition, a tiny crack is formed after the local stress reaches a certain value. Therefore, the density of micro-cracks varies with location and stress. In the damage zone, as illustrated in Fig. 2, the deformation of a position near a micro-crack clearly changes with distance from the macro-crack tip. The coordinate indexes are replaced with numbers as $x_1 \leftrightarrow x$, $x_2 \leftrightarrow y$,$x_3 \leftrightarrow z$.The average strain of damage to the local volume element can be divided into the elastic strain $\bar{\varepsilon}_{ij}^{e}$ in the matrix and the non-elastic strain $\bar{\varepsilon}_{ij}^{c}$ caused by the material defect deformation:

$$\bar{\varepsilon}_{ij} = \bar{\varepsilon}_{ij}^{e} + \bar{\varepsilon}_{ij}^{c}. \tag{14}$$

The matrix elastic strain $\bar{\varepsilon}_{ij}^{e}$ can be calculated based on the constitutive relationship of stress and strain in the undamaged zone. The strain $\bar{\varepsilon}_{ij}^{c}$ of a volume element with many micro-cracks (with total N_α) can be calculated using the micro-mechanics method (Feng and Yu, 2002):

$$\bar{\varepsilon}_{ij}^{c} = \frac{1}{V}\sum_{\alpha=1}^{N_\alpha}\left(\frac{n_i b_j + n_j b_i}{2}\right)^{(\alpha)} dS_\alpha \tag{15}$$

where V is the volume of the representative element and S_α is the surface area of order α micro-crack. Because of the non-uniform distribution of micro-cracks, the selection of the volume and position of the RVE clearly affects the strain value. The deformation of a medium near the crack (α)involves the size and orientation of the crack and the corresponding coordinate transformation (n_j). The displacement of a crack surface (b_k) depends on its geometry and the stress around the crack, and the deformation of the damage zone is closely related to the density of local micro-cracks.

4. Parameters of fracture damage process zone mechanics

4.1. Shape of fracture process zone

The shape of the damage zone near a macro-crack is generally not very regular. Probably, the contour of the damaged area is related to the properties of some materials. Thus, many geometric shapes should be assumed to discuss the deformation and strain of the micro-crack zone. For example, on the basis of the experimental observations by Wang et al. (2008), the width of the damage zone can be designated as a linear distribution with the distance from the macro-crack endpoint, or the damage strip has a semi-elliptical shape. Be based concrete photo-elastic coating experiment by Xu and Reinhardt (1999), and iron specimen strain by Dai et al. (2013), the inelastic region outline before a prefabricated macro crack, is between straight line and ellipse curve. As shown in Fig. B1, that is

$$h(\xi) = h_0\xi/\Gamma, \quad (0 \le \xi \le \Gamma) \tag{16}$$

$$h(\xi) = h_0\sqrt{1 - (\xi - \Gamma)^2/\Gamma^2}, \quad (0 \le \xi \le \Gamma) \tag{17}$$

Here, h_0 is the maximum width of the damage zone and is generally found at the junction of the macroscopic smooth crack and damage zone. Therefore, δ can be estimated by combining Eqs. (9), (15) and (16) or (17).

4.2. Parameters of micro-crack damage zone

For the fracture process zone, the RVE can be assumed to be a cube body with characteristic length $\hat{l}$, width h, and thickness B for the damage strip. For Eq. (15), micro-cracks should be considered as penetrating-type cracks with thickness B in the plane problem. Then, the inelastic strain of the damage zone in the direction perpendicular to the axis of the damage strip should be the projection of $\bar{\varepsilon}_{ij}^{c}$ onto the y -direction:

$$\bar{\varepsilon}_{22}^{c} = \frac{1}{\hat{l}Bh(\xi)}\sum_{\alpha=1}^{N_\alpha}\int_{S_\alpha}\left(\frac{n_i b_j + n_j b_i}{2}\right)_y^{(\alpha)} d(Ba_\alpha) = \frac{1}{h(\xi)\hat{l}}\sum_{\alpha=1}^{N_\alpha}\int_{S_\alpha}(n_2 b_2)^{(\alpha)} d(a_\alpha) \tag{18}$$

where a_α is the perimeter of the intersection curve of the penetration crack and plate plane; $\hat{l}$ is the length of the volume element in the x -direction, which is longer than the average length ($2\hat{a}$) of a micro-crack; b_2 is two times the opening displacement of one side surface of a micro-crack; and "n_2" is the direction cosine of a crack in the y-direction. Considering Eq. (13) and Fig. 2, the characteristic area A^* can be calculated based on the upper and lower opening displacements of a single crack. For a center crack with length $2a$ under uniaxial tension field σ, the area can be determined using the following equation:

$$A^* = \int_{-a}^{a} 2.v_l(x,o)dx = \frac{\sigma 2\pi a^2}{E^*} \tag{19}$$

Here, $E^* = E$ and $E^* = E/(1-\nu^2)$ correspond to the plane-stress and plane-strain states, respectively. Then, the following equation can be obtained:

$$\sum_{\alpha=1}^{N_\alpha}\int_{S_\alpha}(n_2 b_2)^{(\alpha)} d(a_\alpha) = \hat{A}^* N' \tag{20}$$

where the number of equivalent cracks is denoted by N'. Therefore, there is an equivalent characteristic area $\hat{A}^* = 2\pi\sigma.a^2/E^*$. In the macroscopic framework, the formula for the FCOD of the damage zone can be derived as follows, referring to Eq. (9):

$$\delta(\xi) = h(\xi)\bar{\varepsilon}_{22}^{c} = \frac{\hat{A}^* N'(\xi)}{\hat{l}} = \sigma(\xi)\frac{2\pi\hat{a}^2}{E^*\hat{l}}N'(\xi) \tag{21}$$

Here, $\hat{a}$ is the half-length of an equivalent crack. Eq. (21) clearly demonstrates that the FCOD is related to the size and density of micro-cracks.

4.3. Estimation of damage factor and micro-crack density

As shown in Fig. 1, $\varepsilon^e = \sigma/E_0$, which is only confined to the plane-stress state in this paper. Accounting for the interaction of micro-cracks with each other, the Young's modulus of the damage zone with micro-cracks is that for the damage state. That is, $E^* = E_0(1-D)$. If the stress of a point in the fracture process zone is designated as $\hat{\sigma}(\xi) = \sigma$, inputting Eq. (21) into Eq. (11) would give the following equation for D:

$$D(\xi) = \frac{\delta(\xi)E_0}{\bar{\sigma}(\xi)h(\xi) + \delta(\xi)E_0} = \frac{2\pi\hat{a}^2 N'(\xi)}{(1-D)\hat{l}h(\xi) + 2\pi\hat{a}^2 N'(\xi)} \tag{22}$$

In addition, for the RVE with damage, the number of effective micro-cracks $N'(\xi)$ can be calculated using the formula for D. Thus, the solution is

$$N'(\xi) = \frac{\hat{l}h(\xi)}{2\pi\hat{a}^2}D(\xi) \tag{23}$$

In turn, D can be expressed as

$$D(\xi) = \frac{2\pi\hat{a}^2(\xi)}{\hat{l}h(\xi)}N'(\xi) \tag{24}$$

As shown in Eqs. (23) and (24), the distribution of micro-cracks in the fracture process zone is related not only to the damage variable but also to the geometric parameters of the micro-crack. The geometric parameters include the average micro-crack length $2\hat{a}$, the width of the damage zone h, and the character length $\hat{l}$ of the RVE. Because the equivalent crack length may vary with position, $\hat{a} = \hat{a}(\xi)$, in the above formulae. However, using Taylor's composite media method, the interaction of components can be neglected; thus, the zone near a micro-crack can be considered as an undamaged medium. Assuming $E^* = E_0$ in Eq. (21) and inputting this expression into Eq. (11), the number of equivalent continuous micro-cracks can be determined:

$$N''(\xi) = \frac{\hat{l}h(\xi)D}{2\pi\hat{a}^2(1-D)} \tag{25}$$

There is a singularity for N'' in Eq. (25), when $D \to 1$, which is irrational. Regarding the above formula and Eq. (22), there is one more multiplier $(1/(1-D))$ in Eq. (25) than in Eq. (23).

If the equivalent number of micro-cracks is divided by the unit volume of the RVE body, the micro-crack density per unit volume of the damaged zone can be estimated as follows:

$$q(\xi) = \frac{N'(\xi)}{\hat{l}h(\xi)B} = \frac{D(\xi)}{2\pi B\hat{a}^2} \tag{26a}$$

$$\text{Or } D(\xi) = 2\pi B\hat{a}^2(\xi)q(\xi) \tag{26b}$$

From Eqs. (26a,b), it can be observed that the micro-crack density of the damage zone $q(\xi)$ is proportional to the damage factor $D(\xi)$, but inversely proportional to the square of the average micro-crack length ($\hat{a}^2$).

For Eqs (26a,b), if there is a row of micro crack in some segment of damage strip, two micro cracks with same length $\hat{a}$ is substituted for a micro-crack with $2\hat{a}$ length, the damage factor should be became to twice of that. It can be known that micro-crack extension is more dangerous than new micro-crack emerging. No matter the occurrence of micro-cracks or micro-crack growth, they are related to the encircling stress. The occurrence of a micro-crack is often associated with some initial defect in material, and SIF of a micro-crack is proportion to its surrounding stress $\hat{\sigma}$. If some micro-crack extension is hindered when its stress increasing, the damage factor should be limited. Or, when the damage width $h(\xi)$ is increasing with loading, while the micro-crack density of damage strip is not increasing, and probably increasing the materials toughness. So, the Eqs. (26a,b) can be applied analyzing materials structure failure.

5. Experimental observations and calculation example

5.1. Observation of micro-cracks generated during fracture process with loading

Cast iron was selected as the experimental material, as it is a commonly used quasi-brittle material in engineering applications. The material was cut into tensile test specimens of 12-mm length, 4–6-mm width, and 1–2-mm thickness, as shown in Fig. 3(a). A gap with a length of 0.5–2 mm was made on one side of the middle of each specimen perpendicular to the tensile direction using a line-cutting machine. The notched crack width was approximately 0.2 mm. After grinding and polishing the specimen surface, a strain gage with specifications of approximately 1 mm was pasted in the middle of the bottom of the test piece. Then, the specimen was

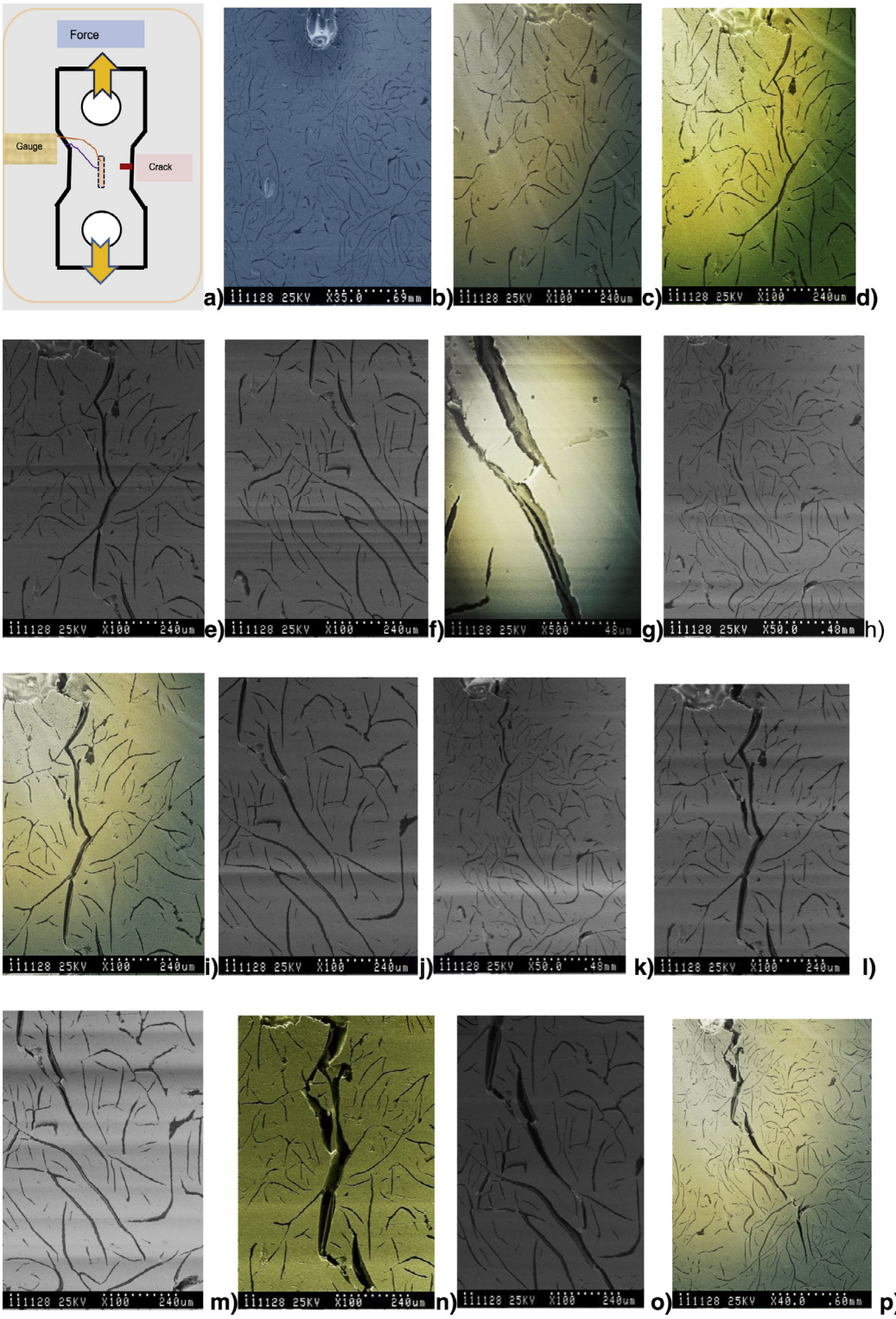

Fig. 3. (a) Schematic illustration of the tensile test specimen. SEM images of cast iron for tensile forces of (b) 0, (c)200, (d) 294, (e)–(g) 356, (h)–(j) 360, (k)–(m) 372, (n)–(o) 394, and (p) 404 N.

placed into a scanning electron microscope (SEM, S570) for observation during a tensile test. During the tensile loading, the SEM operation was controlled by implementation of displacement, and the tensile force and strain were read on a computer screen. When the load or strain reached a certain value, the load was maintained, and multiple images were captured. The corresponding location of the materials differed in the images, and the SEM magnification was not constant. For the measurement of the material deformation under different loads and states, the SEM images were printed out for comparison with an image of the unloaded state with the assistance of the photo-size scale in the microscopy system.

Fig. 3 presents 15 SEM images with tensile forces ranging from 0 to 404 N. The images were captured at the ligament of a prefabricated crack or in the damage process zone. In Fig. 3, the dam-

Table 1
Data of SEM Experiment for the tension of iron specimen with cast crack.

Force (*N*)	200	262	287	294	356	360	372	394	404
FPZ length (mm)	0	0.35	1.32	7.2	13.2	13.6	14.3	18.7	19.8

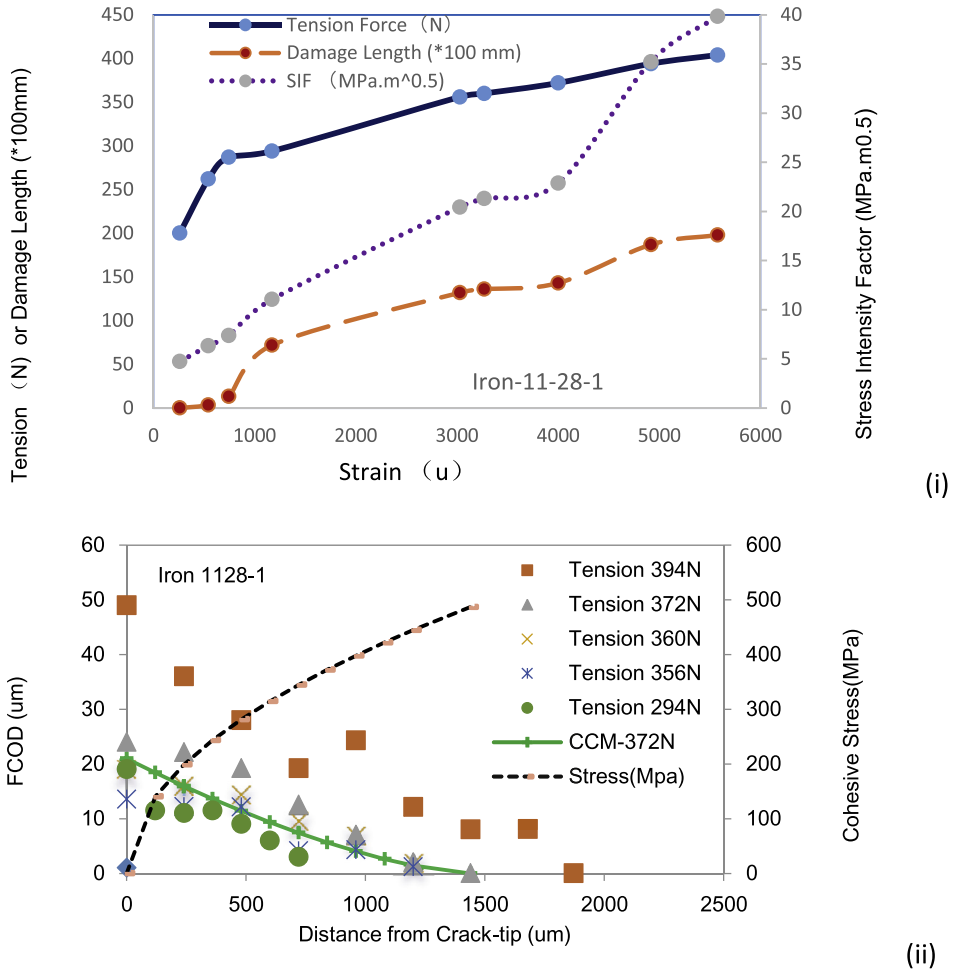

Fig. 4. Experimental data of the loading process. (i) Curves of tensile loading, damage zone length, and SIF as a function of strain. (ii) Curves of FCOD as a function of the distance of the damage zone from the crack tip.

age of the micro-crack first appeared close to the prefabricated gap, and the damage area formed a strip. The deformation of the graphite sheet defect was gentle when the tensile force was less than 300 N. The damage zone was nearly vertical to the tensile direction, and the length of the damage strip increased with increasing tensile loading. The SEM images demonstrate that micro-cracks often appeared on some graphite impurity of the stress concentration. In the low-stress region of the specimen, the deformation near graphite defects was very small, and no micro-cracks were detected. On the stretching process of iron plate with prefabricated crack, the tension force loaded on the specimen and damage length at the crack tip are listed in Table 1. Where, both of FPZ length and tension force are increasing monotonously, and more test data or calculated parameters are shown in Fig. 4.

Fig. 4 presents plots of the tensile force and damage zone deformation of a specimen as a function of strain. In Fig. 4(i), the horizontal coordinate is the micro-strain (10^{-6} or u), and the left vertical coordinate is the "tensile force (N)" (or damage length (mm) $\times$100). The strain and damage zone length of the specimen generally showed a monotonic increase with increasing tension strain.

In Fig. 4(ii), the horizontal axis is the distance from the damage zone to the prefabricated crack tip. On the left vertical ordinate, the relative displacement of both sides in the damage strip or the FCOD under different loadings is presented. In Fig. 4(ii), five tensile force states are shown. Because the micro-crack deformation was not regular when the specimen was near fracture, such as for the tensile force of 404 N, the corresponding curve is not presented. Regardless of the force, the relative displacement of both sides of the damage band gradually decreased with increasing distance of the damage zone from the pre-notched crack tip.

5.2. Fracture parameters under different loading states

For the numerical calculation example, as shown in Fig. 3(a), the limited width plate was loaded with the uniaxial tensile force (T) with width w, thickness b, and crack length a on one side of the plate. The cut crack was perpendicular to the tensile direction. When the stretching stress is σ (equal to $T/(wb)$), the stress intensity factor (SIF) of a type-I crack in plate can be determined using the following equation (Tada et al., 2000):

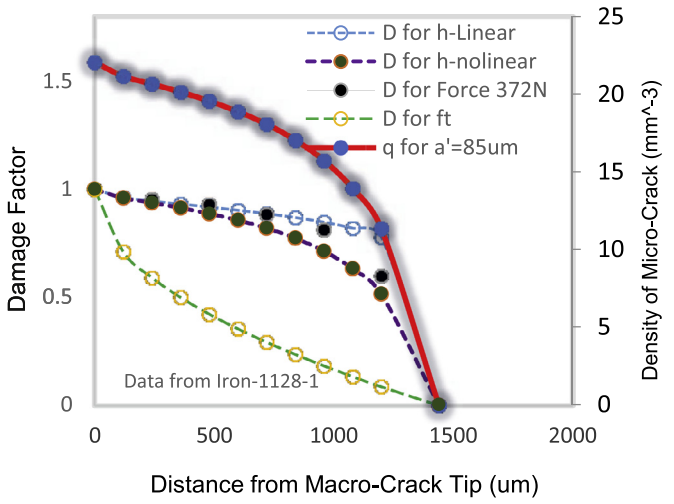

Fig. 5. Distribution of damage factor and micro-crack density of RVE with distance from the fabricated crack tip in the damage zone.

$$K_{\mathrm{I}} = \sigma\sqrt{\pi a}\Big[0.265(1-a/w)^4 + (0.857+0.265a/w)/(1-a/w)^{3/2}\Big] \tag{27}$$

When the damage strip expands in front of the incision, the length of a in the SIF equation should be the total length of the initial crack length and the damage extension length. Fig. 4(i) presents a curve of the change in SIF with varying deformation. The SIF value has units of MPa.m$^{0.5}$ or "Mpa.m^0.5″ and is expressed along the right vertical coordinate of the diagram. SIF monotonically increased with increasing load.

Without loss of generality, the specimen was loaded into a state, e.g., tensile force = 372 N, which resulted in SIF = 22.85 (Mpa.m^0.5) and a damage zone length of approximately 1.43 mm. In addition, the elastic modulus without damage was $E_0 = 87$.Mpa. These parameters were substituted into Eqs. (8a,b); then, the FCOD and cohesive stress of the damage zone were determined, as marked by the continuous dotted line in Fig. 4(ii). The FCOD is plotted on the left vertical coordinate (labeled as "CCM-372N"), and the "cohesive stress" is plotted on the right vertical coordinate as "stress (MPa)." Compared with the opening displacement of the test data shown as discrete "triangle" symbols in Fig. 4(ii), the numerical calculation results in Eqs. (8a,b) are generally consistent with the experimental data obtained using SEM. The cohesive stress distribution in the cutting mouth was almost zero, and the maximum stress of 487 MPa appeared at the end of the damaged zone. The maximum stress was much greater than the tensile strength of general cast iron and was generally close to the ultimate tensile stress of low-carbon steel without damage (Ashby et al., 2008).

5.3. Damage variable and micro-crack density

As the degree of damage in the fracture process zone varies with position, some parameters of the specimen with a tensile force of 372 N could be used to calculate the damage factor in Eq. (11). A value of $E_0 = 87$Mpa was used for the Young's modulus of the material, and the thickness of the damage zone $h(\xi)$ was determined using Eq. (16) or (17). The cohesion stress $\hat{\sigma}(\xi)$ and fictitious crack opening displacement $\delta(\xi)$ were calculated using Eqs. (8a) and (8b), respectively. The resulting $D(\xi)$ values are plotted in Fig. 5, where the left coordinate shows the damage factor $D(\xi)$. "D for h-linear" represents the value of $h(\xi)$ obtained using Eq. (16), and "D for h-nonlinear" corresponds to the data obtained using Eq. (17).

In Fig. 5, the solid points for "D for Force 372 N" represent the damage factor calculated using Eq. (11), and the displacement determined using SEM, and $h(\xi)$ was calculated using Eq. (17). To facilitate comparison, the value of the damage factor calculated using Eq. (12), which was based on the ultimate stress of the material, is presented along the left vertical axis of Fig. 5 with the legend "D for ft." Fig. 5 clearly shows that the experimental data and results obtained using Eq. (17) were closer to the test data and differed from the "D for ft" data in terms of the ultimate tensile stress. Therefore, it is not appropriate to calculate the damage variable for cast iron material using the ultimate tensile stress. The damage factor always decreased with increasing distance from the prefabricated crack tip, gradually changing from close to 1 to 0. As shown in Fig. 5, at macro crack tip, the damage factor equal to 1 meaning that the material is completely disconnected, so the disconnection order can be expected by the curves of damage factor.

From Eqs. (26a,b), it is clear that the change of the micro-crack density $\boldsymbol{q}$ varies with the damage factor in the fracture process zone. As shown in Fig. C1, the length of micro crack is variable in the damage strip of iron tension specimen. The maximum and minimum lengths are 0.135(mm) and 0.241(mm) respectively, but the lengths of some micro crack are randomly distribution as Fig. C1(a,b). If $2\hat{a} = 170$ (um) and $h_0 = 0.456$ mm are assumed, the density of the micro-crack of RVE can be determined using Eq. (26a), and the result is shown as the right vertical coordinate of Fig. 5. The curves of the micro-crack density in Fig. 5 are labeled "q for a' = 85 um". As observed in this figure, there may be twenty or more micro-cracks per mm^3. The micro-crack density was small near the no damage zone. However, this type of continuity function obtained using the homogenization method only reflects the relative relationship between the density of micro-crack, and damage variable.

6. Discussion and conclusion

For quasi-brittle materials, the relationship between the stress and deformation of micro-cracks in the damage process zone in front of a macroscopic gap can be evaluated by combining the homogenization method in meso-mechanics and the cohesive crack model of nonlinear fracture. By Eqs. (8a,b), the cohesive stress and opening displacement of a damage strip are calculated with giving the materials elastic modulus, length of the damage strip and the SIF of far loaded. When the cracked material structure is in the state of balance, the SIF is also the resistance SIF. So, the SIF is less or equal to the instability toughness of its materials ($K_{\mathrm{Ic}}^{\mathrm{un}}$).

On the basis of the damage factor defined from the concept of an effective bearing cross section and a function of the mechanics parameters in the damage zone, the damage degree can be expressed as a function of position in the fracture process zone. The damage factor variable is closely related to the width distribution of the fracture process zone with micro-cracks. Eqs. (26a,b) express that damage factor is proportional to the density of micro-crack in damage zone, and is also proportional to the square of micro-crack length. As the damage factor (D) is between 0 and 1, and for $D = 1$ or $D = D_c$ (criterion damage factor) display a statue of complete fracture or failure, then, damage factor is related to fracture toughness. So, it is known that the damage degree in the damage strip is related not only to the density of micro-cracks, the cohesive stress distribution, but also to the geometrical factors of micro-cracks in the FPZ strip.

Acknowledgments

This work was supported by The State Key Laboratory of Nonlinear Mechanics in the Institute of Mechanics of Chinese Academy Sciences (Grant No: 2011-12-13), and National Natural Science

Foundation of China (Grant No: 10272068, 50438010). The first author would like to thank Mr. Li Duanyi, Mr. Xie Jijia, Ms. Duan Guihua, and QUT students Ms. Chen Ting, and Ms. Geng Hui for their help on the experimental works in the LNM of the Institute of Mechanics, China. The authors would like to thank the reviewers and editor for their valuable comments on the manuscript, and Enago (www.enago.cn) for the English language review.

Appendix A. Analytical solution of the cohesive crack model

A1. Integral solution of the cohesive crack model

As shown in Fig. A1, as a non-elastic band is located at the end of a smooth crack, the segment is regarded as a fictitious crack or cohesive crack segment. The non-elastic area is surrounded by an elastic area with deformation and stress in the area for a type-I fracture problem. If the fracture mechanics concept of a smooth crack is adopted here, cohesive stress and fictitious crack opening displacement occur along the cohesive crack. The FCOD distribution is expressed as a polynomial with different powers of the distance from the cohesive end (Wang et al., 2006):

$$\delta = \frac{4\Gamma}{E\pi}\sum_{n=1}^{N} C_n\left(\frac{\xi}{\Gamma}\right)^{n-1/2}, \quad (0 \le \xi \le \Gamma). \tag{A1}$$

In fact, the FCOD is formed by the stress K field and crack cohesion stress. On the basis of the superposition principle of solid mechanics, $\delta = \delta_K + \delta_\sigma$ as shown in the following equations:

$$\delta_K = \frac{8K_I}{E}\sqrt{\frac{\xi}{2\pi}}, \quad (0 \le \xi \le \Gamma), \tag{A2a}$$

$$\delta_\sigma = \frac{4}{E\pi}\int_0^\Gamma \sigma(\eta)\ln\left|\frac{\sqrt{\xi}+\sqrt{\eta}}{\sqrt{\xi}-\sqrt{\eta}}\right| d\eta, \quad (0 \le \xi \le \Gamma). \tag{A2b}$$

In addition, this equation can be reduced to a Fredholm-type integral equation. If $\chi = \xi/\Gamma$, we obtain

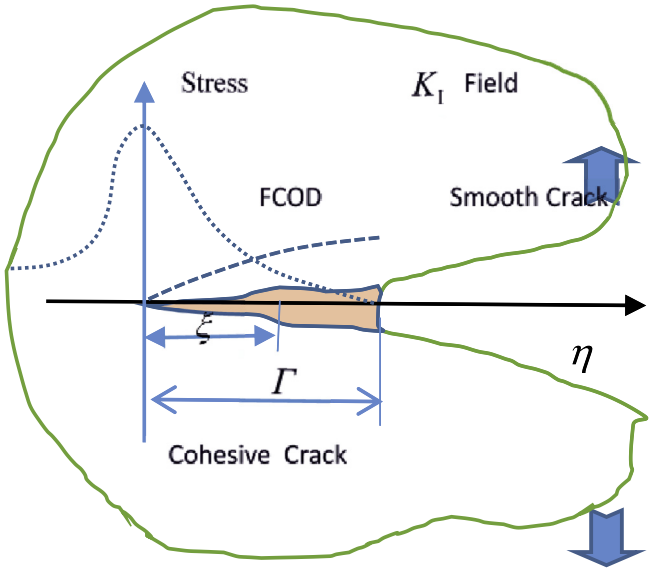

Fig. A1. Schematic diagram of the cohesive crack model.

$$\int_0^1 \sigma(\theta)\ln\left|\frac{\sqrt{\chi}+\sqrt{\theta}}{\sqrt{\chi}-\sqrt{\theta}}\right| d\theta = K_I\sqrt{\frac{2\pi\chi}{\Gamma}} - \sum_{i=1}^{N} C_i(\chi)^{i-1/2}, \quad (0 \le \sqrt{\chi} \le 1). \tag{A3}$$

The cohesive stress solution to the above equation is:

$$\sigma(\xi) = \frac{1}{\sqrt{2\pi}}\frac{K_I}{\sqrt{\Gamma-\xi}} + \sum_{n=1}^{N}\frac{-C_n}{2\pi\Gamma}\sqrt{\frac{\Gamma}{\Gamma-\xi}}\left(\sum_{r=0}^{n-1}\frac{2^{-2r}(2r)!}{(r!)^2}\left(\frac{\xi}{\Gamma}\right)^{n-r-1}\right) + \sum_{n=2}^{N}\frac{C_n}{\pi}\sqrt{1-\frac{\xi}{\Gamma}}\left(\sum_{r=0}^{n-2}\frac{2^{-2r}(n-r-1)(2r)!}{(r!)^2}\left(\frac{\xi}{\Gamma}\right)^{n-r-2}\right) \quad (0 \le \xi \le \Gamma), \tag{A4}$$

Where, C_n (n = 1, 2,...N) are undetermined parameters.

A2. Elimination of stress singularity and calculation of undetermined parameters

For the distribution of cohesive stress, there are stress singularities at the two ends of the cohesive crack segment. To eliminate the stress singularities, it is required that $\sigma\sqrt{\xi} \to 0$ when $\xi \to 0$ and $\sigma\sqrt{\Gamma-\xi} \to 0$ when $\xi \to \Gamma$. Using the Lagrange multiplier method, two equations for the elimination of stress singularities are introduced in the energy functional of the cohesive crack. On the basis of the variational principle,

$$\delta\Pi = \sum_{j=1}^{N+2}\frac{\partial\Pi}{\partial C_j}\delta C_j. \tag{A5}$$

Regarding the undetermined parametersC_j of the FCOD distribution, the following set of algebraic equations can be obtained:

$$\sum_{i=1}^{N} A_{ij}C_i + C_{N+1} + A_{j0}C_{N+2} = A_{1j}K_I\sqrt{\frac{2\pi}{\Gamma}}, \quad (j = 1, 2, \ldots, N), \tag{A6a}$$

$$C_1 + \frac{3}{2}C_2 + \frac{15}{8}C_3 + \ldots + \sum_{r=0}^{N-1}\frac{2^{-2r}(2r)!}{(r!)^2}C_N + 0.C_{N+1} + 0.C_{N+2} = K_I\sqrt{\frac{2\pi}{\Gamma}}, \quad (j = N+1), \tag{A6b}$$

$$A_{10}C_1 + A_{20}C_2 + \ldots + A_{N0}C_N + 0.C_{N+1} + 0.C_{N+2} = [2A_{10} - 1]K_I\sqrt{\frac{2\pi}{\Gamma}}, \quad (j = N+2). \tag{A6c}$$

Wang et al. (2006) had determined A_{ij} using calculus:

$$A_{10} = 1/2, A_{11} = 1/4, A_{20} = A_{30} = \ldots = 0, A_{12} = A_{21} = A_{22} = 3/16, A_{23} = A_{32} = A_{33} = 45/256, \text{ and } A_{1(N+1)} = 1, \ldots..$$

Using Eq. (A6c), we can obtain$C_1/2 = 0$. Referring to Eq. (A6b), for $N = 2$, we have

$$C_1 = 0; \; C_2 = \frac{2K_I}{3}\sqrt{\frac{2\pi}{\Gamma}}. \tag{A7a,b}$$

When inputting Eq. (A7) into Eqs. (A1), (A4), (8a,b) in the main text are obtained. For $N = 3$, the relation curves of FCOD and stress are not smooth and contain oscillations (Zhang et al., 2012).

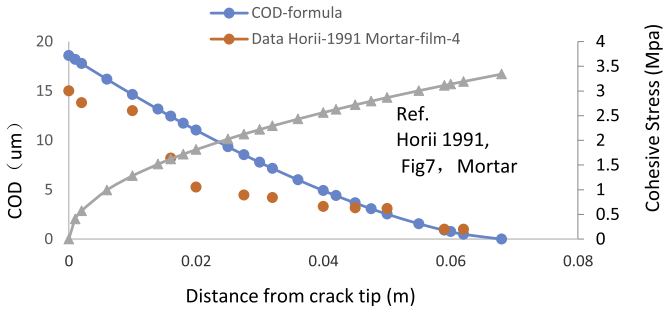

Fig. A2. The distribution of COD and Stress in cohesive crack model is correlated to the observation of FPZ by laser speckle technique.

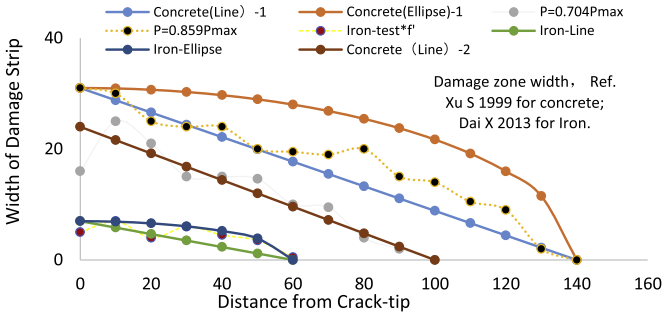

Fig. B1. The width of damage strip for concrete and iron.

A3. The opening displacement and stress of cohesive crack model correlated to test date

Consulting Eqs. (A1), (A4) and (A7a,b) above, the COD and stress of cohesive crack model can be worked out by Eqs. (8a,b) in the text, if the FPZ length (Γ), SIF of far loaded (K_I), and elastic modules (E) are given. By laser speckle technique, Horii and Ichinomiya (1991) got the opening displacement of cohesive crack in tension specimen of mortar or concrete. From Fig. 7 in the reference for mortar, the data of COD is shown in the left vertical axis of Fig. A2 in this paper. For $\Gamma = 0.68$(mm), $K_1 = 1.092$Mpa(m)^0.5, $E = 32.6$Mpa, the COD(um) and Stress (Mpa) can be calculated by Eqs. (8a,b), and are shown in Fig. A2 for continuous curves. Where, the horizontal axis indicates the distance from the macro crack tip, and cohesive stress is shown in the right vertical axis.

From Fig. A2, it is known that the opening displacement curve is basically consistent with the curve profile of test data by laser speckle technique. The maximum value of cohesive stress distribution is approached to the ultimate tensile strength ($f_t \cong 3.4$Mpa). By comparing the calculation results of Eqs. (8a,b) with tested data (Horii and Ichinomiya, 1991), it shows that the theoretical model is valid.

Appendix B. Width of damage strip contour at the tip of a macro crack

It is all known that the contour of fracture process zone is a long strip for quasi-brittle materials as concrete and iron. By photo-elastic coating, Xu and Reinhardt (1999) obtained the distributions of principal strain on concrete. For the contours of strain (noted 0.45) of concrete, in Ref. Fig. 16, for $P = 0.704P$max and $P = 0.859P$max, the width of FPZ is expressed in Fig. B1. The horizontal axis indicates the distance from the macro crack tip, with 'mm' unit, and the contour width is shown in the vertical axis of Fig. B1. As to iron material, Dai et al. (2013) obtained the contour of damage strip. By multiplied by pixel conversion coefficient f', the contour data from Fig. 15 of reference, is also expressed in Fig. B1 of this paper.

The distribution of damage strip width can be calculated for parameters h_0 and Γ, by Eqs. (16) and (17). As to concrete material, $h_0 = 31$(mm), 24(mm); $\Gamma = 140$(mm), 100(mm) are set respectively, and the calculation curves are shown in Fig. B1. For the iron material, the reference parameters $h_0' f' = 7$(mm) and $\Gamma' f' = 60$(mm) are set, and the contour curves of line and ellipse are also shown in the same figure.

From Fig. B1, it is known that the points of experiment data are between the curves of ellipse and straight ling, especially for data

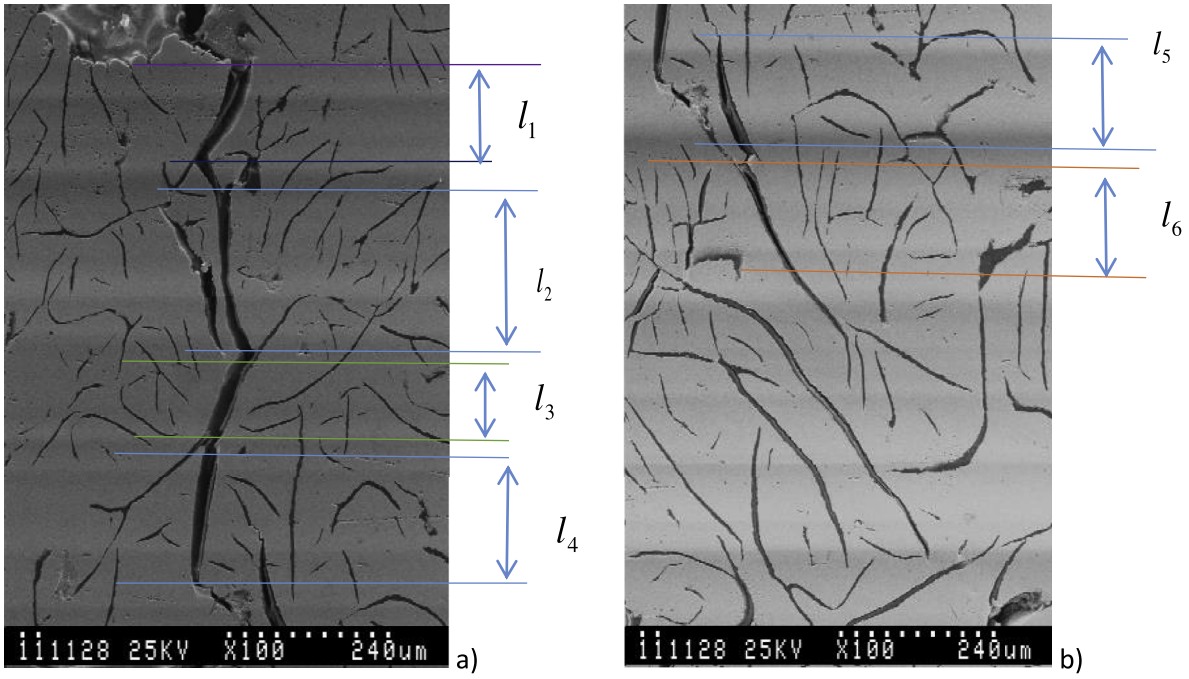

Fig. C1. The micro crack length in the damage strip of iron specimen, it is perpendicular to the tension direction of specimen at tension force 372(N).

with "$P = 0.859$Pmax" and "Iron-test*f'". This is reason the ellipse and straight line are supposed as the contours of damage zone, for Eqs. (16) and (17).

Appendix C. The length of micro-crack of iron in damage strip

For the photos of Fig. 3(l,m) in this text, the lengths of micro cracks are measured by the photo ruler. The length is the dimension in perpendicular to the tension direction of iron specimen. As shown in Fig. C1, six cracks length are got respectively. There are, $l_1 = 136$(um), $l_2 = 241$(um), $l_3 = 135$(um), $l_4 = 199$(um), $l_5 = 174$(um), $l_6 = 136$ (um). The average value of equivalent crack length is 170 (um), or its half is a' = 85(um).

References

Ashby, M., Shercliff, H., Cebon, D., 2008. Materials: Engineering, Processing and Design. Elsevier Inc, Beijing China.

Bouvard, J.L., Chaboche, J.L., Feyel, F., Gallerneau, F., 2009. A cohesive zone model for fatigue and creep–fatigue crack growth in single crystal superalloys. International Journal of Fatigue 31, 868–887.

Boyce, B.L., Kramer, S.L.B., Fang, H.E., Cordova, T.E., 2014. The Sandia Fracture Challenge:blind round robin predictions of ductile tearing. Int. J. Fract. 186, 5–68.

Carpinteri, A., Cornetti, P., Puzzi, S., 2006. Scaling laws and multiscale approach in the mechanics of heterogeneous and disordered materials. Appl. Mech. Rev. 59, 283–304.

Cyron, C.J., Marigo, Jean-J., Sicsic, P., 2014. Cohesive model approach to the nucleation and propagation of cracks due to a thermal shock. Int. J. Fract. 187, 51–75.

Dai, X., Yang, F., Wang, L., Zhang, D., Pu, Q, He, X., 2013. Load capacity evaluated from fracture initiation and onset of rapid propagation for cast iron by digital image correlation. Optics and Lasers in Engineering. 51 20131992-1101.

Feng, X., Yu, S., 2002. Damage Micromechanics of Quasi-brittle Materials. Higher Education Press, Beijing China. (In Chinese).

Gao, Y.C., 1989. Damage theory of materials with microstructure. Act. Mech. Sin. (5) 136–144.

Hashin, Z., Shtrikman, S., 1962. On some variational principles in anisotropic and non-homogeneous elasticity. J. Mech. Phys. Solids. 10, 335–342.

Hertzberg, W.R., 1996. Deformation and Fracture Mechanics of Engineering Materials. John Wiley & Sons Inc, New York, U.S.A.

Hillerborg, A., Modeer, M., Petersson, P.E., 1976. Analysis of crack formation and crack growth in concrete by means of fracture mechanics and finite element. Cem Conc. Res. 6 (6), 773–782.

Horii, H, Ichinomiya, T, 1991. Observation of fracture process zone by laser speckle technique and governing mechanism in fracture of concrete. Int. J. Fract. 51, 19–29.

Huang, Y., Yang, S.Q., Tian, W.L., Zeng, W., Yu, L.Y., 2016. An experimental study on fracture mechanical behavior of rock-like materials containing two unparallel fissures under uniaxial compression. Act. Mech. Sin. 32 (3), 442–455.

Krajcinovic, D., 1984. Continuum damage mechanics. Appl. Mech. Rev. 37, 1–6.

Lemaitre, J., Chaboche, J.L., 1990. Mechanics of Solid Materials. Cambridge University Press, Cambridge U. K.

Li, S.F., 1998. Introduction to Micromechanics and Nano-mechanics. University of California, Berkeley, USA..

Pichler, B., Dormieux, L., 2007. Cohesive zone size of micro-cracks in brittle materials. Eur. J. Mech. A/Solids 26, 956–968.

Pichler, B., Dormieux, L., 2009. Instability during cohesive zone growth. Eng. Fract. Mech. 76, 1729–1749.

Pichler, B., Hellmich, C., 2010. Estimation of influence tensors for eigen-stressed multiphase elastic media with nonaligned inclusion phases of arbitrary ellipsoidal shape. J. Eng. Mech. (ASCE). 136 (8), 1043–1053.

Polyanin, A.D., Manzhirov, A.V., 1998. Handbook of Integral Equation. CRC Press, USA.

Roth, S., Hütter, G., Kuna, M., 2014. Simulation of fatigue crack growth with a cyclic cohesive zone model. Int. J. Fract. 88, 23–45.

Shackelford, J.F., 2000. Introduction to Materials Science for Engineers, 5th edition Prentice Hall, New Jersey of U.S.A.

Shen, W., 1995. Damage Mechanics. Huazhong University of Science and Technology Press, Wuhan China In Chinese.

Shen, Y., 2002. Integral Equation. The Press of Beijing Institute of Technology, Beijing China (In Chinese).

Smith, E., 1994. The elastically equivalent softening zone size for an elastic-softening material: I. Power law softening behavior.. Mech. Mater. 17, 363–368.

Tada, H., Paris, P.C., Irwin, G.R., 2000. The Stress Analysis of Cracks Handbook. ASME Press, New York. U.S.A.

Wang, L., Sun, M., et al., 2008. Electronical measurement of fracture process of cast iron incision specimen and calculation of the structure bearing capacity. Act. Metal. Sin. 44 (7), 853–858 In Chinese.

Wang, L., Xu, S., Zhao, X., 2006. Analysis of cohesive crack opening displacement considering strain softening effet. Science China. Series G 49 (1), 88–101.

Wei, Y., Qiu, X., Hwang, K.C., 2004. Steady-state crack growth and fracture work based on the theory of mechanism-based strain gradient plasticity. Eng. Fract. Mech. 71, 107–125.

Xu, S., Reinhardt, H.W., 1999. Determination of double-K criterion for crack propagation in quasi-brittle fracture. Part I. II. and III,. Int. J. Fract. 98 (2), 111–193.

Yang, W., Lee, W.B., 1993. Mesoplasticity and Its Applications. Springer-Verlag, Berlin.

Yao, W., Zhang, Z., Hu, X., 2015. Jordan form asymptotic solution near the tip of a V-shaped notch in Reissner plate. Int. J. Solids Struct. 75-76, 225–234.

Zhang, D., Wang, L., Yun, H., Shen, Y., 2012. Opening displacement and stress distribution of cohesive crack in cast iron. J. Mech. Strength 34 (1), 126–130 In Chinese.

Zhang, Y., Zhang, Z., 2008. Mesomechanics of Materials. Science Press of China, Beijing PR China In Chinese.

Zhan, S., Wang, T., Han, X., 1999. Analysis of two-dimensional finite solids with microcracks. Int. J. Solids Struct. 36, 3735–3753.

Zhou, C., Li, K., 2015. Transport properties of concrete altered by crack-induced damage. J. Mater. Civil Eng. 27.